




# A finite element model to predict the double hearing protector effect on an in-house acoustic test fixture

Yu Luan,<sup>1,a)</sup>  Franck Sgard,<sup>2</sup> Hugues Nélisse,<sup>2</sup> and Olivier Doutres<sup>1</sup>

<sup>1</sup>Department of Mechanical Engineering, École de Technologie Supérieure, 1100 Rue Notre-Dame Ouest, Montreal, Quebec H3C 1K3, Canada

<sup>2</sup>Direction Scientifique, IRSST, 505 Boulevard de Maisonneuve Ouest, Montreal, Quebec H3A 3C2, Canada

## ABSTRACT:

The sound attenuation of double hearing protectors (DHPs), earplugs combined with earmuffs, generally falls short of the sum of each single protector's attenuation when used independently. This phenomenon, referred to as the DHP effect, is found to be related to structure-borne sound transmission involving the outer ear and can also be observed on acoustic test fixtures (ATFs). At present, it still remains not fully understood, and no available model can help demonstrate the associated sound transmission mechanisms. In this work, a finite element model is proposed to study the DHP effect on an ATF between 100 Hz and 5 kHz. Power balances are calculated with selected configurations of the ATF in order to (i) quantify the contribution of each sound path, and study the effects of (ii) the artificial skin and (iii) acoustic excitation on the ATF exterior boundaries. The DHP effect is shown to originate from the structure-borne sound power injected from the ATF boundaries and/or earmuff cushion. The important influence of earcanal wall vibration is highlighted when the skin is accounted for. The simulation results allow for gaining more insight into the sound transmission through a DHP/ATF system.

© 2022 Acoustical Society of America. <https://doi.org/10.1121/10.0009835>

(Received 20 July 2021; revised 2 March 2022; accepted 4 March 2022; published online 18 March 2022)

[Editor: James F. Lynch]

Pages: 1860–1874

## I. INTRODUCTION

Double hearing protectors (DHPs), namely, earplugs combined with earmuffs, shall be used to protect workers in high noise level environments.<sup>1</sup> However, it is generally recognized that their sound attenuation is difficult to predict due to the occurrence of the DHP effect.<sup>2</sup> The latter refers to the phenomenon where the overall sound attenuation achieved by the DHP falls short of the algebraic sum of every single protector's attenuation when used independently. This effect was first observed in DHP attenuation measurements on human subjects<sup>3–6</sup> and was attributed to certain sound paths that bypass the hearing protectors: (i) the sound transmitted through the head and body directly to the middle and inner ears at frequencies above 2 kHz<sup>3,4</sup> (middle and inner ear bone conduction paths), and (ii) the acoustical and mechanical couplings between the earplug and earmuff<sup>5,6</sup> or the occlusion effect<sup>7</sup> contributing to the energy in the earcanal at frequencies below 2 kHz (outer ear bone conduction path). However, the exact contribution of the outer ear path to the DHP effect appeared to be ambiguous.

More recently, Nélisse *et al.*<sup>8</sup> found that the DHP effect also occurs when DHP attenuation measurements are carried out on acoustic test fixtures (ATFs). These authors characterized the DHP effect by the decrease in the earplug noise reduction (NR) after adding an earmuff. Following the work of Nélisse *et al.*, the authors of the present paper have

conducted a series of specially designed experiments to measure the earplug NRs without and with an earmuff on a commercial ATF by controlling the sound pressure level (SPL) under the earmuff.<sup>2</sup> These experiments suggested that the DHP effect is mainly related to the outer ear structure-borne (SB) sound transmission induced by external acoustic excitation. More specifically, this effect occurs when the contribution to the energy in the earcanal of the SB sound paths outweighs that of the airborne (AB) path due to the low SPL at the earcanal entrance compared to the single earplug configuration. According to the convention used, the AB path refers to the direct sound transmission into the earcanal through the earmuff, air cavity under the earmuff and earplug, while the SB paths refer to all the other sound paths through the hearing protectors and ATF. By excluding the importance of several potential SB paths which originate from the earmuff headband and ATF tripod, and focusing on the outer ear because of the use of an ATF, the authors suggested that the DHP effect on the ATF could be attributed to the SB paths involving (i) the mechanical coupling between the earplug and earmuff *via* the earmuff cushion/ATF assembly and (ii) the vibration of the earcanal walls, which is similar to the fundamental mechanisms of the occlusion effect on human subjects. However, the respective contribution of each sound transmission path has not been identified yet.

Numerical modeling, as it has been done for single hearing protectors,<sup>9–12</sup> remains a useful approach for gaining more insight into the sound transmission mechanisms through the DHP. Nevertheless, to the best of the authors'

<sup>a)</sup>Electronic mail: [yu.luan.1@ens.etsmtl.ca](mailto:yu.luan.1@ens.etsmtl.ca)

knowledge, no numerical model of the DHP/human head system can be found in the literature in view of the complexity of the system. The only existing DHP/ATF numerical models based on the finite element (FE) method could not even reproduce the tendency of experimental measurements due to an omission of the mechanical coupling between the earplug and earmuff *via* the ATF<sup>8</sup> or an incomplete consideration of the SB sound paths in the system.<sup>13</sup> A comprehensive literature review on both the experimental and numerical studies of DHP sound attenuation is available in the authors' previous work.<sup>2</sup>

This paper is a continuation of the authors' experimental analysis on the DHP effect.<sup>2</sup> Its main objective is to propose a FE model in order to (i) study the DHP effect characterized by the difference between the NRs of an earplug alone and in a DHP on an ATF and (ii) better understand the sound transmission mechanisms through the DHP. First, a FE model of a DHP/ATF system is built following the modeling strategies proposed for a single earplug<sup>9,10</sup> and a single earmuff.<sup>11,12</sup> Particularly, as the constitution of the earmuff cushion is complex and its most advanced model is accompanied with difficulties in assessing the mechanical properties,<sup>12</sup> it is replaced by a silicone cushion of identical shape. Additionally, since the outer ear SB paths play an important role in the sound transmission through the DHP, an in-house ATF with a geometry simpler than a commercial one is used to better account for essential components in the model. The simulation results based on the FE model are then compared with the NR measurements of the single earmuff, single earplug and earplug in the DHP in a reverberant room. Finally, in order to quantify the contribution of each sound transmission path considered and study the effects of the system construction, such as its material properties and boundary conditions, the FE model is exploited to calculate the power balances using selected configurations of the in-house ATF.

The paper is organized as follows. Section II describes the FE modeling strategy for the DHP/ATF system and simulation configurations, along with the geometry, boundary

conditions, material properties, and the selected acoustic and vibratory indicators. Section III presents the experimental measurements of the hearing protector sound attenuation. Finally, Sec. IV analyzes and discusses the simulation and measurement results for different configurations of interest.

## II. FINITE ELEMENT MODELING OF THE DHP/ATF SYSTEM

### A. Geometry

The system of interest is a DHP worn on an in-house ATF (see Fig. 1). The in-house ATF consists of an instrumented circular steel plate. It has a similar weight but a much simpler geometry compared to the G.R.A.S. 45CB ATF (G.R.A.S. Sound & Vibration AS, Denmark) used in the authors' previous work.<sup>2</sup> As explained in the introduction, this design makes it possible to better account for the SB sound transmission through the system in the FE model. In addition, simple boundary conditions can be chosen for the corresponding setup to facilitate their application in the model. Inside the in-house ATF, a cylindrical earcanal has been drilled whose size is identical to the one in the G.R.A.S. 45CB. In contrast to commercial ATFs specified in the standard ANSI S12.42,<sup>14</sup> certain simplifications have been made to the in-house ATF. First, the pinna simulator and artificial skin layer in the earcanal are not included. Second, there is no built-in temperature control unit. Third, the acoustic impedance produced by the ear simulator<sup>15</sup> in the earcanal is not accounted for. Moreover, as the focus is put on the outer ear, the middle and inner ears are not included either. Actually, the terminal surface of the in-house ATF earcanal has been designed to correspond to the "eardrum position" in a commercial ATF earcanal where sound pressure is recorded.<sup>16</sup> More specifically, an internal miniature microphone together with a microphone holder is tightly attached to the ATF so that the microphone is flush-mounted into the holder at the "eardrum position." A small cylindrical air cavity lies behind the microphone for passing its wire. These components may still contribute to the sound

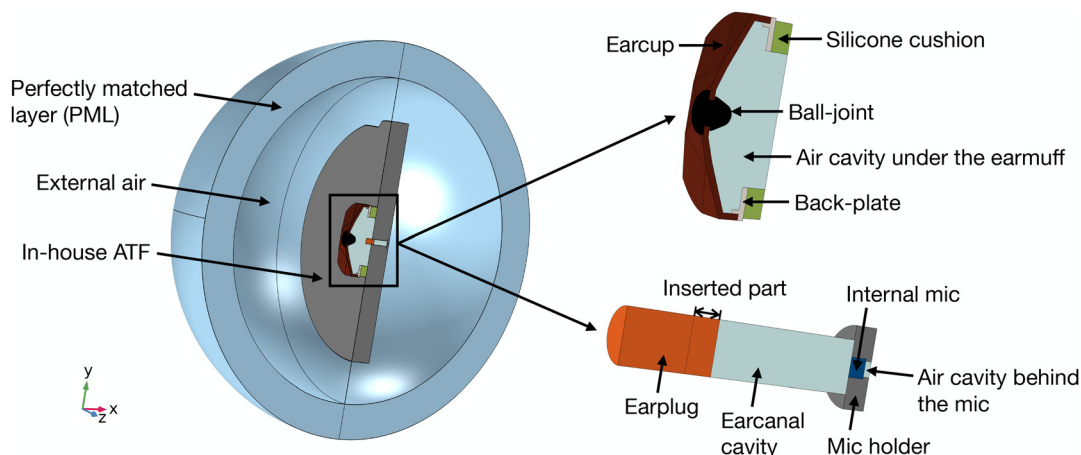


FIG. 1. (Color online) Geometry of the DHP/ATF system (symmetric view): global view (left); earmuff with a silicone cushion (upper right); earplug inserted into the earcanal (lower right).

TABLE I. Key geometric dimensions of the components in the FE model.

	ATF	Mic holder	Internal mic	Cavity behind the mic	Open earcanal
Outer radius/radius (mm)	170	5.75	1.4	1.1	3.75
Thickness/length (mm)	30.1	3.6	2.6	1	26.5
	Occluded earcanal	Silicone layer	Silicone pad	Cushion	Earplug
Outer radius/radius (mm)	3.75	5.75	57.5	—	3.75
Thickness/length (mm)	22.5	14	10	10.6	14

pressure in the earcanal cavity but mimicking a realistic contribution of the eardrum together with the middle and inner ears is not within the scope of the present paper.

The studied DHP consists of an earplug made of silicone rubber specially molded to fit the shape of the in-house ATF earcanal and a commercial earmuff (EAR-MODEL-1000, 3 M<sup>TM</sup> E-A-R<sup>TM</sup>, Indianapolis, USA) as used for the experiments in the authors' previous work.<sup>2</sup> Such types of single hearing protectors have already been studied numerically and experimentally.<sup>9–12</sup> The total length of the earplug is 14 mm and the length of the inserted part is 4 mm, which corresponds to a shallow insertion.<sup>17</sup> The radius of the earplug is chosen to be 3.75 mm which is identical to that of the earcanal but in practice, its actual radius is slightly larger

in order to ensure a good sealing condition (see Sec. III). The foam liner inside the air cavity under the earmuff is not taken into consideration as it does not significantly modify the vibratory behavior of the system. As justified in the introduction, the original comfort cushion of the earmuff is replaced by a silicone cushion of identical shape. The thickness of the compressed silicone cushion assessed *in situ* when the earmuff is worn on the ATF is about 10.6 mm. Key geometric dimensions of the system components are provided in Table I.

Two configurations of the in-house ATF are mainly studied through FE models. The first one, referred to as ATF#1 [see Fig. 2(a)], corresponds to the original ATF structure built to carry out experimental measurements as

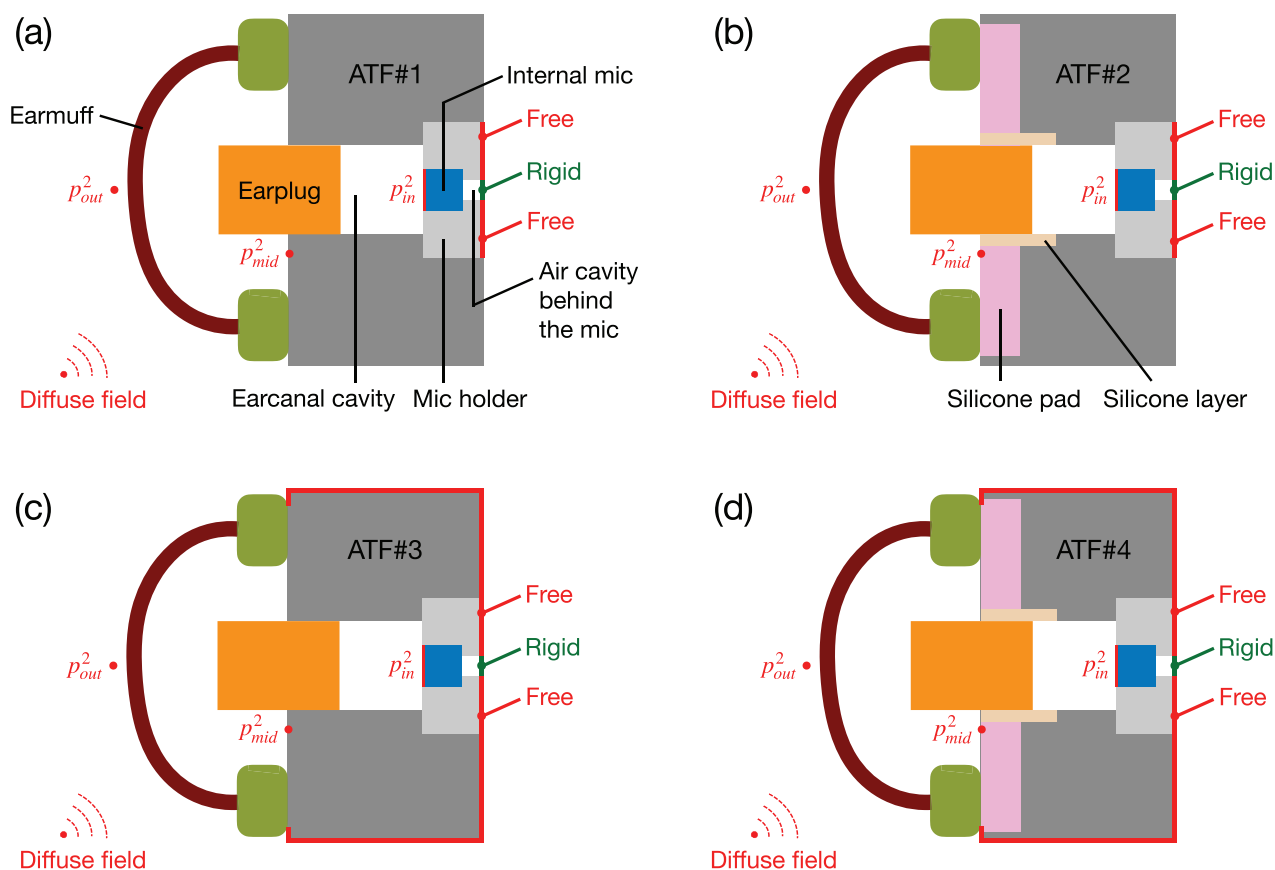


FIG. 2. (Color online) Schematic representation of the DHP worn on (a) fully “rigid” ATF#1 and (b) ATF#2 with artificial skin portions (cross section view). (c) ATF#3 and (d) ATF#4 are similar to ATF#1 and ATF#2, respectively, but their exterior boundaries outside the earmuff are decoupled from the external air domain as indicated by a thick red line.

depicted in Fig. 1. It does not include skin mimicking portions, and its earcanal lateral walls are considered to be “rigid.” The second modeled ATF, referred to as ATF#2 [see Fig. 2(b)], is similar to ATF#1 but a silicone layer and a silicone pad mimicking the skin portions in contact with respectively the interior of the earcanal and earmuff cushion are accounted for. Their geometric dimensions are similar to the artificial skin parts of a commercial ATF and can also be found in Table I. The use of ATF#2 makes the system more realistic in terms of material properties and allows for investigating the influence of the skin on the DHP effect. Additionally, complementary ATF configurations, namely, ATF#3 and ATF#4 have also been investigated numerically [see Figs. 2(c) and 2(d)], and are explained in Sec. II B.

## B. Loading, coupling, and boundary conditions

For each configuration of the in-house ATF, the simulated DHP/ATF system is supposed to be placed inside an infinite external air domain. It is modeled with an air-filled convex domain surrounded by a perfectly matched layer (PML)<sup>18</sup> which simulates the Sommerfeld condition (see Fig. 1). The system is excited by a diffuse sound field modeled as a superposition of incoming uncorrelated plane waves with equal amplitude freely propagating in multiple directions in the external air domain. Each incident plane wave with direction of propagation described by the elevation angle  $\theta \in [0, \pi]$  and azimuthal angle  $\varphi \in [0, 2\pi]$  (in the yz plane, see Fig. 1) can be written as

$$p(\theta, \varphi) = 0.3 \exp(-j(k_x x + k_y y + k_z z)), \quad (1)$$

with  $k_x = k_0 \cos \theta$ ,  $k_y = k_0 \sin \theta \cos \varphi$ ,  $k_z = k_0 \sin \theta \sin \varphi$ , and  $k_0$  the wavenumber. The amplitude of 0.3 Pa ensures that the overall SPL in the model is approximately the same as that measured in the room during the experiments (see Sec. III). Continuity of stresses and displacements is assumed at the interfaces between solid domains. At fluid-solid interfaces, the fluid-structure coupling condition applies, i.e., continuity of tractions and normal displacements. The FE formulations associated with the problem of interest are classic and are not recalled here for the sake of conciseness. The reader can, for example, refer to Chapters 3 and 6 of Atalla and Sgard<sup>19</sup> for details.

For ATF#1, decoupled conditions are applied to the back surface of the air cavity behind the internal microphone and that of the microphone holder [see Fig. 2(a)]. More specifically, an acoustically rigid boundary condition is imposed at the interface between the air cavity behind the microphone and external air domain; the microphone holder's exterior surface, which is in contact with the external air domain, is considered to be free. In other words, no acoustic excitation is applied to these boundaries. This condition is assumed to correspond to the setup used for the experiments. For ATF#2, the same decoupled conditions are adopted for the purpose of comparison [see Fig. 2(b)]. Particularly, ATF#3 and ATF#4 [see Figs. 2(c) and 2(d)] are similar to ATF#1 and ATF#2, respectively, but all the

exterior boundaries of the ATF outside the earmuff are considered to be decoupled from the external air domain. These two configurations allow for studying the influence on the DHP effect of the acoustic excitation on the ATF exterior boundaries. Again, note that ATF#1 has been physically fabricated to carry out experimental measurements to verify the corresponding FE model, while ATF#2–ATF#4 are simulated configurations. They are all identical in terms of ATF size and earcanal geometric dimensions.

## C. Material properties

The air domains (external air, air cavity under the earmuff, earcanal cavity, and air cavity behind the internal microphone) are modeled as compressible perfect gas domains, defined by their density ( $\rho_0 = 1.2 \text{ kg/m}^3$ ) and speed of sound ( $c_0 = 343.4 \text{ m/s}$ ) under standard conditions for temperature ( $T_0 = 293.15 \text{ K}$ ) and atmospheric pressure ( $P_0 = 1.01e^5 \text{ Pa}$ ). No energy losses are accounted for in the external air domain, while the dissipation induced by thermo-viscous effects in the air cavity under the earmuff is considered using a structural loss factor of 1%.<sup>11,12</sup> The thermo-viscous effects in the earcanal cavity and air cavity behind the microphone are calculated based on the low reduced frequency model of a circular duct type.<sup>20</sup> In this model, thermal and viscous losses are distributed homogeneously in the bulk of the fluid through a complex wavenumber and characteristic impedance. It requires much less computational resources compared to a full thermo-viscous acoustic model based on the linearized Navier-Stokes equations.

The earcup and back-plate of the earmuff are made of Acrylonitrile Butadiene Styrene (ABS), and its ball-joint is made of rubber.<sup>11,12</sup> In addition, the in-house ATF and microphone holder are made of steel, and the internal microphone is made of aluminum. These components together with the artificial skin parts are modeled as linear isotropic elastic solids whose mechanical properties are given in Table II. Particularly, the properties of artificial skin are adopted from Viallet *et al.*<sup>10</sup>

The mechanical properties of the earplug and silicone cushion are characterized using cylindrical specimens on a quasi-static mechanical analyzer (QMA)<sup>21</sup> and calibrated according to the sound attenuation measurements of single protectors. The earplug is modeled as a linear isotropic elastic solid<sup>10</sup> and its properties can also be found in Table II. Specifically, the silicone cushion is considered as a linear isotropic viscoelastic solid. Its frequency dependent Young's modulus and loss factor are assessed using a method similar to that proposed by Boyer *et al.*<sup>11</sup> by means of curve fitting a fractional derivative Zener model based on the low frequency QMA data obtained with cylindrical specimens (see the Appendix).

## D. Meshing and solving

All the domains in the FE model are meshed using 10-noded tetrahedral elements except for the PML domain which is meshed using 15-noded quadratic triangular



TABLE II. Mechanical properties of the components in the FE model.

	ATF/mic holder	Internal mic	Silicone (artificial skin)	Earcup/back-plate	Ball-joint	Cushion	Earplug
$\rho_s$ (kg/m <sup>3</sup> )	7850	2700	1150	1200	800	1170	1500
$E_s$ (GPa)	200	70	$4.2 \times 10^{-4}$	2.16	0.1	—	$2.9 \times 10^{-3}$
$\nu_s$ (1)	0.3	0.33	0.43	0.38	0.48	0.49	0.49
$\eta_s$ (1)	0.005	0.005	0.2	0.05	0.5	—	0.1

prisms. In vibroacoustic applications, a convergence criterion of at least four elements per wavelength is commonly accepted in order for the mesh to capture the system response.<sup>19</sup> In this paper, a criterion of six elements per wavelength is selected. Preliminary simulations by refining the meshes have shown that this criterion is sufficient for achieving the desired accuracy of the solution, e.g., difference of about 0.5 dB in the SPL at the “eardrum position” of ATF#2 at 5 kHz when the criterion is changed from four elements to six elements per wavelength. For calculating the acoustic and vibratory indicators under a diffuse field excitation, the system equations are solved for each incident plane wave in the software COMSOL MULTIPHYSICS (v.5.6 COMSOL®, Sweden). Each diffuse field indicator can then be calculated through an integration over the entire space,

$$A^d = \int_0^{2\pi} \int_0^\pi A_{(\theta,\varphi)} d\theta d\varphi, \quad (2)$$

with  $A_{(\theta,\varphi)}$  being a mean square sound pressure or an exchanged power described in Sec. II E. In the present paper, the diffuse field indicators are all computed based on a Gauss point integration scheme of 16 Gauss points.<sup>22</sup> Simulations are carried out in narrow frequency bands from 100 Hz to 5 kHz with a resolution of 20 Hz to limit the computation time.

## E. Calculation of acoustic and vibratory indicators

### 1. Sound attenuation indicators

Mean square sound pressures are computed at three different locations (see Fig. 2) for each incident plane wave in the FE model: (i) at a point outside but close to the center of the earcup ( $p_{out}^2$ ), (ii) at a point below but close to the earcanal entrance ( $p_{mid}^2$ ), and (iii) at the surface of the internal microphone, i.e., at the “eardrum position” ( $p_{in}^2$ ). These locations approximately correspond to the real microphone positions in the experiments (see Sec. III). The associated diffuse field results  $p_{out}^d$ ,  $p_{mid}^d$ , and  $p_{in}^d$  are then derived from Eq. (2) in order to determine the sound attenuation indicators of the hearing protectors. In the following equations [see Eqs. (3)–(5)], the abbreviations “EM” (single earmuff), “EP” (single earplug), and “DHP” (DHP configuration) are used in the superscripts.

As explained in the introduction, the NRs of the earplug alone ( $NR_{EP}$ ) and in the DHP configuration ( $NR_{EP}^{DHP}$ ) are of particular interest for quantifying the DHP effect.<sup>2</sup> They are defined as the difference between the SPLs at the earcanal

entrance and at the “eardrum position” when a single earplug [see Eq. (3)] or a DHP [see Eq. (4)] is worn,

$$NR_{EP} = 10 \log_{10} \left( \frac{p_{mid}^{d,EP^2}}{p_{ref}^2} \right) - 10 \log_{10} \left( \frac{p_{in}^{d,EP^2}}{p_{ref}^2} \right), \quad (3)$$

$$NR_{EP}^{DHP} = 10 \log_{10} \left( \frac{p_{mid}^{d,DHP^2}}{p_{ref}^2} \right) - 10 \log_{10} \left( \frac{p_{in}^{d,DHP^2}}{p_{ref}^2} \right), \quad (4)$$

where  $p_{ref} = 2 \times 10^{-5}$  Pa. In particular, the NR of the earmuff alone ( $NR_{EM}$ ) is also calculated using ATF#1. It corresponds to the difference between the SPLs outside the earmuff and at the “eardrum position” when a single earmuff is worn,

$$NR_{EM} = 10 \log_{10} \left( \frac{p_{out}^{d,EM^2}}{p_{ref}^2} \right) - 10 \log_{10} \left( \frac{p_{in}^{d,EM^2}}{p_{ref}^2} \right). \quad (5)$$

### 2. Exchanged powers

In order to quantify the energy transfers through the DHP/ATF system, the powers exchanged at the interfaces between different fluid and solid domains are calculated. At a fluid-solid interface, for example at the earplug medial surface towards the earcanal cavity, the exchanged power can be calculated by

$$\Pi_{exch,f/s} = \frac{1}{2} \Re \left[ \int_S p \vec{n} \cdot \vec{v}^* dS \right], \quad (6)$$

where  $\Re$  denotes the real part of the quantity,  $p$  is the sound pressure in the fluid domain,  $\vec{v}^*$  denotes the complex conjugate of the structural velocity, and  $\vec{n}$  the normal vector to the interface. At a solid-solid interface, such as the interface between the earplug and earcanal lateral walls, the exchanged power is expressed as

$$\Pi_{exch,s1/s2} = \frac{1}{2} \Re \left[ \int_S \underline{\underline{\sigma}} \vec{n} \cdot \vec{v}^* dS \right], \quad (7)$$

where  $\underline{\underline{\sigma}}$  denotes the structural stress tensor. In addition, the power dissipated in a solid domain due to structural damping can be calculated by

$$\Pi_{diss,s} = \frac{1}{2} \Re \left[ -j\omega \int_V \underline{\underline{\sigma}} : \underline{\underline{\varepsilon}}^* dV \right], \quad (8)$$

where  $\underline{\underline{\sigma}} : \underline{\underline{\varepsilon}}^*$  refers to the double dot product of the structural stress tensor and the complex conjugate of the structural

strain tensor. The corresponding diffuse field powers  $\Pi_{exch,f/s}^d$ ,  $\Pi_{exch,s1/s2}^d$  and  $\Pi_{diss,s}^d$  are obtained using Eq. (2) by substituting Eqs. (6)–(8) for  $A_{(\theta,\varphi)}$ . Finally, the diffuse field power dissipated in a fluid domain due to thermo-viscous effects is calculated using a power balance approach. The power balance for a given fluid domain writes

$$\sum \Pi_{exch,f/s}^d + \Pi_{diss,f}^d = 0. \quad (9)$$

### III. EXPERIMENTAL SETUP

The sound attenuation indicators of the hearing protectors (see Sec. II E 1) are measured at normal room temperature using the setup corresponding to ATF#1 (see Fig. 3). Measurements are carried out in a diffuse sound field generated by four loudspeakers (MACKIE® HD1531) placed at each corner of a reverberant room (approximately 8.76 m × 7.77 m × 3.12 m). The speakers are fed with white noise of about 110 dB in overall SPL using a Minirator MR2 audio generator (NTi Audio AG, Liechtenstein). The in-house ATF is suspended on an aluminum frame in the center of the room using nylon cords *via* two hooks on the ATF. The center of the ATF earcanal is located at a height of about 75 cm above the floor. The earplug is shallowly inserted into the earcanal, which facilitates the removal of the earplug. The silicone cushion is attached to the back-plate of the earmuff using strong double-sided adhesive tape. The earmuff together with the silicone cushion is placed on the ATF with the help of a half headband screwed to the ATF. The half headband was already used in Boyer *et al.*<sup>23</sup> to reproduce the clamping force imposed by the span of a standardized commercial ATF of about 11.5 N. The hooks on the ATF and half headband are not included in the FE model in order to simplify the problem and reduce the computational cost. Preliminary simulations using ATF#1 have shown that these components barely affect the earplug NR.

The mean square sound pressure at the “eardrum position” is measured using a miniature microphone (FG-23629-

P16, Knowles®, Itasca, IL) fixed by a microphone holder at the terminal of the ATF earcanal (see Fig. 1, lower right). A small air cavity behind this microphone has been fabricated in the microphone holder to pass the wire of the microphone. The back surface of this air cavity and that of the microphone holder are covered carefully with mounting putty in order to minimize the influence of parasitic sound leaks. In addition, two miniature microphones (FG-23329-D65, Knowles®, Itasca, IL) are attached to (i) the half headband outside the earmuff [see MIC<sub>out</sub> in Fig. 3(b)] and (ii) the ATF front surface close to the earcanal entrance [see MIC<sub>mid</sub> in Fig. 3(c)] to measure the mean square sound pressures at the corresponding positions. Particularly, a narrow groove has been made on the ATF front surface to pass the wire of the microphone positioned at the earcanal entrance (MIC<sub>mid</sub>) to the outside of the earmuff. This groove is filled with mounting putty to avoid potential sound leaks induced by the wire between the silicone cushion and ATF. A reference 1/2 in. microphone (BSWA Technology Co., China) is placed at about 1 m from the earcanal entrance (not shown in Fig. 3) in order to obtain the transfer functions between the other three microphones and this microphone.<sup>10,23</sup> These transfer functions are then substituted for the mean square sound pressures in Eqs. (3)–(5) to calculate the sound attenuation indicators of interest. Tests are performed using respectively the single earmuff, single earplug and DHP. Each test is repeated three times by removing and repositioning the studied hearing protectors in order to account for the variability related to the mounting conditions.

### IV. RESULTS AND DISCUSSION

#### A. Sound attenuation of hearing protectors

##### 1. Model evaluation

First, the simulated sound attenuation of the hearing protectors in both the single and DHP configurations on ATF#1 is compared with the experimental data (see Figs. 4 and 5).

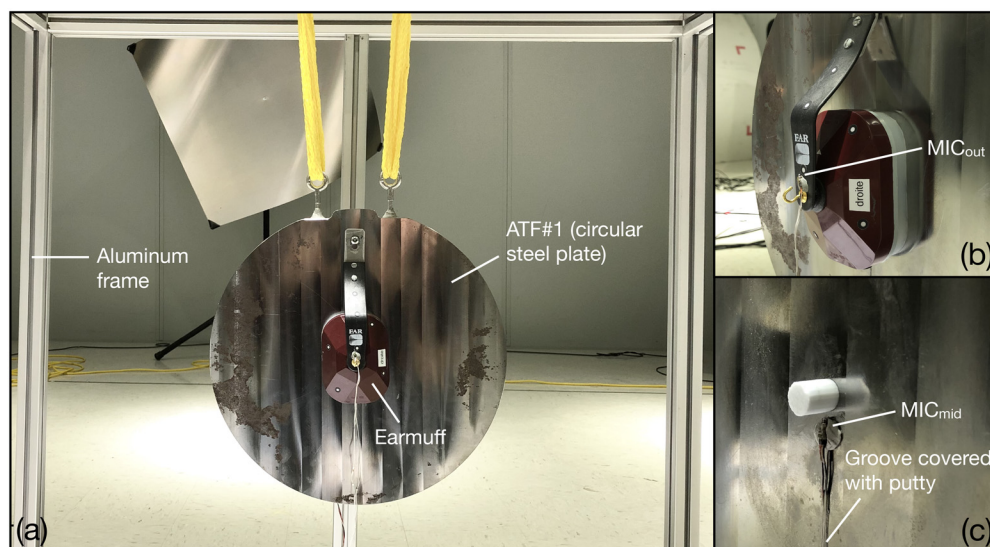


FIG. 3. (Color online) Experimental setup adopted: (a) global view; (b) earmuff with a silicone cushion; (c) earplug inserted into the earcanal.

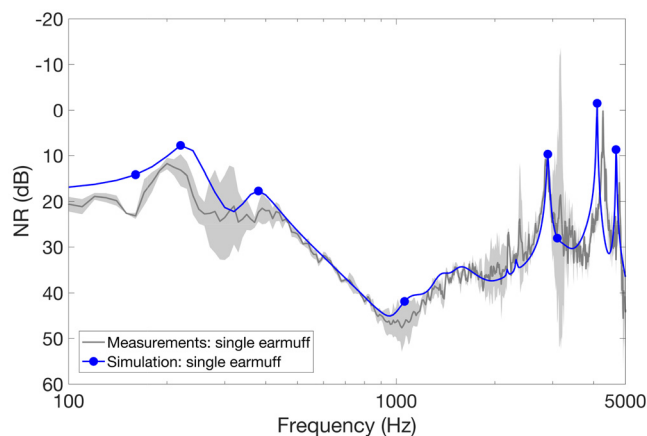


FIG. 4. (Color online) NRs of the single earmuff measured and simulated using ATF#1: measurement results (averaged value with 95% confidence interval, gray zone); broadband simulation result (blue curve with dots highlighting specific frequencies discussed below).

The latter are displayed in terms of mean values and 95% confidence intervals for the three repetitions of each test. Figure 4 presents the single earmuff NRs in which the blue curve with dots and gray zone correspond respectively to the simulation and measurement results.

The figure shows that the simulated earmuff NR is in very good agreement with the experimental data. The earmuff with a silicone cushion is found to be capable of replicating the earmuff pumping motion<sup>23–25</sup> at about 230 Hz. The trough around 380 Hz corresponds to a mechanical mode of the earmuff under acoustic excitation for which (i) the inner and outer lateral walls of the silicone cushion vibrate in phase, and (ii) the rest of the structure moves as a rigid body. A similar phenomenon has been pointed out in past studies which considered the original earmuff comfort cushion as an equivalent elastic solid.<sup>12,24</sup> Some discrepancies are observed between the simulation and measurement

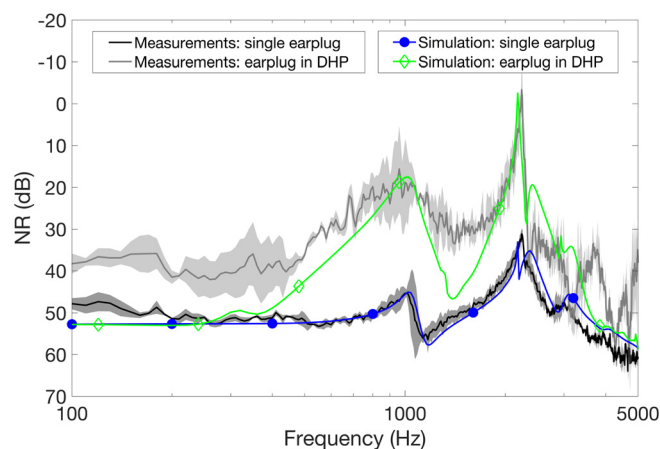


FIG. 5. (Color online) NRs of the earplug measured and simulated using ATF#1: measurement results of the single earplug (averaged value with 95% confidence interval, black zone) and earplug in the DHP (averaged value with 95% confidence interval, gray zone); broadband simulation results of the single earplug (blue curve with dots) and earplug in the DHP (green curve with diamonds).

results at 150–250 Hz and around 1.2 kHz, probably due to the mechanical properties of the silicone cushion that are not accurately captured in these frequency zones controlled by the cushion behavior. Indeed, the silicone specimens used for property characterization are simply cylindrical in shape (see Sec. II C), whereas the cushion is of a more complex shape. At about 3 kHz, a local minimum of the earmuff NR is found. It is related to an acoustic resonance controlled by the earcanal cavity. Particularly, the large variability in the experimental data around 3.2 kHz might be associated with the mounting conditions, such as the asymmetrical compression of the silicone cushion. The latter may modify (i) the direct sound transmission through the cushion walls, (ii) the actual shape of the air cavity under the earmuff and thus the associated acoustic resonances excited. The troughs around 4.1 and 4.7 kHz correspond to the coupled modes of the earmuff controlled by the earmuff cavity.<sup>25,26</sup>

The simulated and measured earplug NRs are compared in Fig. 5. The black and gray zones denote the measured NRs of the single earplug and of the earplug in the DHP. The DHP effect, i.e., difference between the NRs of the earplug alone and in the DHP can be observed up to 5 kHz. This finding confirms the ability of the proposed in-house ATF to capture this effect as already observed on commercial ATFs and human subjects. The blue curve with dots and green curve with diamonds correspond to the associated simulation results respectively. A satisfactory agreement is seen between the simulation and measurement results in the single configuration in nearly the whole frequency range concerned, and in the DHP configuration mainly at frequencies above 400 Hz. In the single configuration, the two earplug modes<sup>27</sup> at about 1 and 2.5 kHz controlled respectively by the longitudinal vibrations of its non-inserted and inserted parts, can be predicted by the FE model. A sharp trough is observed around 2.2 kHz from both the simulation and measurement results. It corresponds to a symmetric bending wave mode of the in-house ATF for which the central region of the ATF exhibits the highest displacement. The earcanal together with the earplug and earmuff all lies within this region. Particularly, in contrast to the measurements, this ATF mode is more clearly distinguished from the earplug second mode in the simulation, maybe because the system overall damping is not well estimated in the related frequency zone. Comparing the DHP configuration to the single configuration, the overall tendency of the DHP effect can also be correctly captured by the model in the frequency range concerned. The most significant DHP effect, up to about 40 dB, occurs at medium frequencies between 2 and 2.5 kHz where the bending wave mode of the ATF is observed. The DHP effect is also found to be pronounced around 1 kHz probably because of the maximum earmuff attenuation that is reached in this frequency range<sup>2</sup> (see also Fig. 4).

At frequencies below 400 Hz, the simulated earplug NRs in both the single and DHP configurations are similar. In other words, no significant DHP effect is shown by the FE model. This observation is consistent with the



experimental data obtained on a commercial ATF in the authors' previous work<sup>2</sup> and on human subjects in Nélisse *et al.*<sup>8</sup> It has been explained by the low earmuff attenuation in this frequency range due to the pumping motion that increases the sound pressure under the earmuff, and makes the direct AB sound path through the earplug outer surface dominant over the SB paths.<sup>2</sup>

However, the measured earplug NRs in the single and DHP configurations are not close to each other below 400 Hz, which suggests a non-negligible DHP effect. In this frequency range, the measured earplug NR in the DHP is lower than the simulated one by up to about 15 dB. Supplementary tests (both experimental and numerical) suggest that this phenomenon could be explained by potential SB sound transmission through the earcanal terminal portion, which is not accurately captured by the model. This behavior might contribute directly to the sound pressure in the earcanal cavity, or facilitate the sound radiation of the earcanal lateral walls without evidently changing the sound pressure at the earcanal entrance, and in turn decreases the earplug NR. As the DHP has a much higher AB attenuation compared to the single earplug, it is more sensitive to SB transmission, and the decrease in the earplug NR is only pronounced in the DHP configuration. Such a phenomenon is also found to have an effect around 1.5 kHz and in several higher frequency bands (e.g., around 3.7 and 4.6 kHz) where differences can be observed between the simulated and measured earplug NRs in the DHP. Moreover, as the AB attenuation of the earmuff is even lower than that of the earplug alone, especially at frequencies below 400 Hz (due to the pumping motion and transverse mode of the silicone cushion previously explained), this phenomenon is not detectable in the case of the earmuff alone (see Fig. 4).

According to the results above, despite some local discrepancies between the simulation and measurements in the DHP configuration, for which the results may be treated with caution, the FE model is deemed capable of capturing the general behavior of the DHP/ATF system at most frequencies where the DHP effect mainly occurs. In the following, numerical analyses are carried out in the frequency range from 100 Hz to 5 kHz since (i) the simulations based on the model are consistent with the measurements on commercial ATFs and human subjects which have shown an important DHP effect only above 400–500 Hz,<sup>2,8</sup> and (ii) the model is mainly exploited to analyze different sound transmission paths, and study the impacts of material properties and boundary conditions on the DHP effect in an ideal system without the influence of undesirable SB sound that can hardly be avoided in practice (see Secs. IV A 2 and IV B).

## 2. Analysis of the contribution of the ATF on the DHP effect

Now the FE model is used to simulate the earplug NRs in the single and DHP configurations on different ATFs of interest [see Fig. 6(a)]. For the purpose of a clearer comparison,  $\Delta NR_{DHP}$  defined as the difference between the NRs of

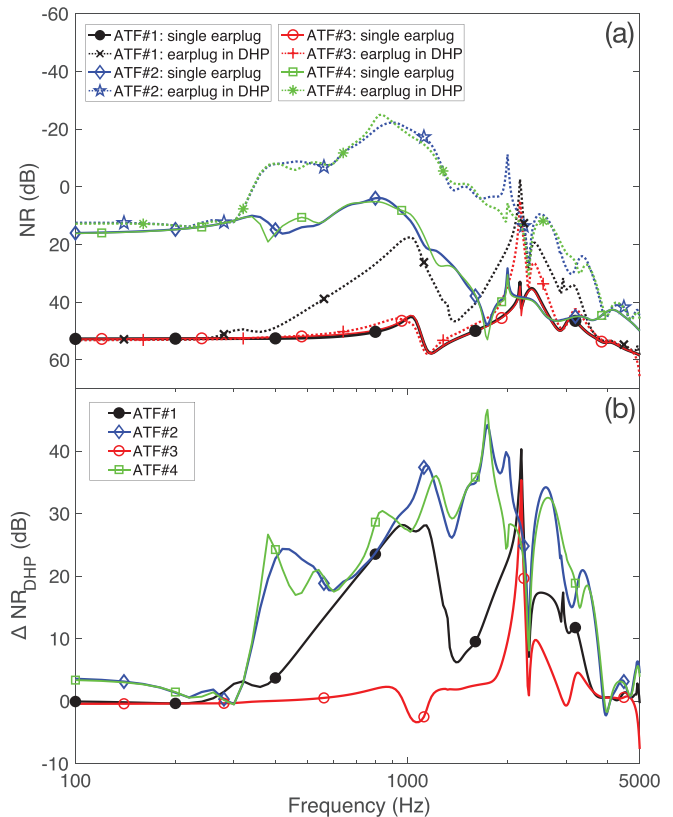


FIG. 6. (Color online) Simulation results of (a) earplug NRs: results of the single earplug on ATF#1 to ATF#4 corresponding to black dots, blue diamonds, red circles and green squares, and results of the earplug in the DHP on ATF#1 to ATF#4 corresponding to dotted black crosses, dotted blue pentagrams, dotted red plus signs and dotted green asterisks; (b)  $\Delta NR_{DHP}$ : results on ATF#1 to ATF#4 corresponding to black dots, blue diamonds, red circles and green squares.

the earplug alone and in the DHP for each ATF (i.e.,  $\Delta NR_{DHP} = NR_{EP} - NR_{EP}^{DHP}$ , see Sec. II E 1) is also displayed in Fig. 6(b). This indicator was already used in the authors' previous work<sup>2</sup> to characterize the DHP effect.

First, the simulation results on ATF#1 and ATF#2 are compared in order to study the impact of the artificial skin on the DHP effect. From a mechanical point of view, the skin plays an important role around the earplug lateral walls which reduces the overall stiffness of the earplug/ATF system. As a result, it is expected to have more sound energy radiated into the earcanal cavity by the earplug and earcanal walls. This explains the significant decrease in the single earplug NR by up to 45 dB on ATF#2 compared to ATF#1 at frequencies below 1.5 kHz where the system is mainly controlled by its stiffness<sup>10</sup> [see Fig. 6(a)]. The lowest single earplug NR on ATF#2 is observed around 800 Hz. This observation could be attributed to multiple coupled modes of the earplug/skin assembly excited in this frequency range. Moreover, compared to ATF#1, the frequency of the symmetric bending wave mode of ATF#2 is slightly reduced to about 2 kHz again due to the inclusion of the artificial skin that decreases the system overall stiffness. It is interesting to mention that both the NRs of the single earplug and of the



earplug in the DHP on ATF#2 are of a similar order of magnitude to the experimental data obtained on human subjects in Nélisse *et al.*<sup>8</sup> This observation indicates the importance of taking into account the skin for predicting the DHP attenuation in a more realistic way.

Figure 6(b) shows that  $\Delta NR_{DHP}$  is close to zero at frequencies below 300 Hz for both ATF#1 and ATF#2. As explained in Sec. IV A 1, the direct AB sound path through the earplug outer surface is dominant over the SB paths in this frequency range due to the pumping motion and silicone cushion transverse mode, which hence decreases the DHP effect. In most frequency bands, the DHP effect on ATF#2 is found to be higher than that on ATF#1. This phenomenon could result from the use of the artificial skin which raises the vibration of the earcanal walls (in contact with the non-occluded part of the earcanal cavity), increases the acoustic volume velocity imposed by the latter, and therefore favors the outer ear SB path.

Second, the results of  $\Delta NR_{DHP}$  are also compared between all the ATFs in order to investigate the influence on the DHP effect of the acoustic excitation on the ATF exterior boundaries [see Fig. 6(b)]. A notable DHP effect on ATF#3 is only observed around 2.2 kHz, where the bending wave mode of the ATF occurs. It is found to be lower than the DHP effect on ATF#1 at most frequencies below 2 kHz and above 2.5 kHz. This means that the acoustic excitation on the ATF exterior boundaries has an important influence in these configurations within the corresponding frequency zones. On the opposite, the comparison between ATF#2 and ATF#4 shows that the acoustic excitation on the ATF boundaries does not make a great difference to the DHP effect when the artificial skin is accounted for. This phenomenon is further studied through power balances in Sec. IV B.

## B. Analysis of the contribution of each sound path using power balances

This section presents the simulation results of power balances. The results for ATF#1 (fully “rigid”) and ATF#2 (with artificial skin) are discussed in the two following subsections, respectively. For each of them, the power balances are calculated in two chosen domains, namely, the earcanal cavity and ATF. The power balances in the earcanal cavity are compared between the single and DHP configurations. This comparison makes it possible to study the relative contributions of different sound paths without and with the earmuff. The power balances in the ATF are shown only for the DHP configuration for which SB sound transmission is considered to be significant. The main sources of the SB paths in the system are then identified. The power balances in the earplug are also calculated. For the sake of conciseness, these results together with the simulated power balances for ATF#3 and ATF#4 are included in Appendix B in the supplementary material.<sup>28</sup>

### 1. ATF#1: Fully “rigid” ATF

Figure 7 illustrates the calculated power balances in the earcanal cavity of ATF#1. Figures 7(a) and 7(b) represent the single earplug and DHP configurations respectively. Numbers 1–4 denote the power spectra levels exchanged between the earcanal cavity and (1) the earplug medial surface, (2) the earcanal lateral walls, (3) the earcanal terminal surface, and (4) the power spectrum level dissipated in the earcanal cavity due to thermo-viscous effects. In the following figures of power balances, a solid curve indicates an amount of power flowing into a domain of interest (e.g., earcanal cavity for Fig. 7) through an associated boundary,

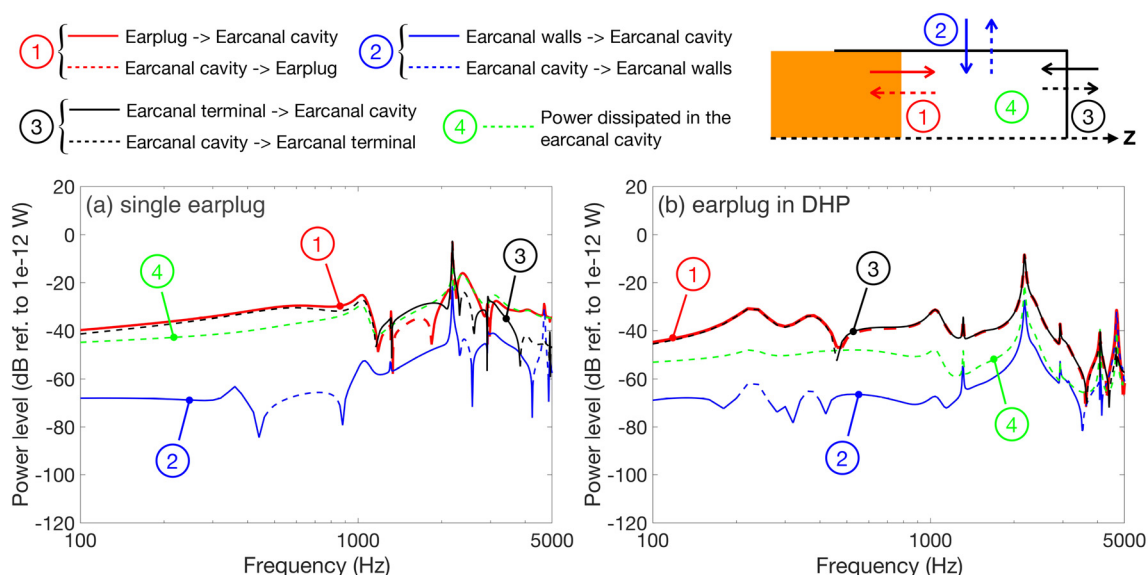


FIG. 7. (Color online) Power balances in the earcanal cavity of ATF#1 for (a) single earplug configuration and (b) DHP configuration: power spectra levels exchanged at the earplug/earcanal cavity interface (red); exchanged at the earcanal lateral walls (blue); exchanged at the earcanal terminal surface (black); dissipated in the earcanal cavity (green). Numbers 1–4 correspond to the associated geometric zones where the powers are calculated. Solid line, power flowing into the earcanal cavity; dashed line, power flowing out of (or dissipated in) the earcanal cavity.

while a dashed curve indicates the power flowing out of (or dissipated in) this domain.

For most frequency bands in the single earplug configuration [see Fig. 7(a)], the direct AB sound transmission is dominant. More specifically, most power is injected into the earplug through its outer surface in contact with the external air domain [see also Fig. B.1(a) in the supplementary material<sup>28</sup>], and flows into the earcanal cavity due to the sound radiation of the earplug medial surface (solid red curve). The highest sound radiations of the earplug around 1 and 2.5 kHz are related to its modes (see Sec. IV A 1). This part of power is either dissipated internally (dashed green curve), or flows out of the earcanal cavity through the earcanal terminal surface (dashed black curve). At certain frequencies (i.e., around 1.3, 2.2, and 2.9 kHz), the earcanal terminal surface is found to inject power into the earcanal cavity (solid black curve). These frequencies correspond to different bending wave modes of the ATF. Additional simulations of mechanical fluxes (not presented here) show that these modes facilitate the vibration transmission from the ATF to the microphone holder and thus the sound radiation from the latter into the earcanal cavity. The mode at 2.2 kHz contributes the most to the injected power since it leads to the highest displacement within the central region of the ATF (see Sec. IV A 1). The contributions of the other modes are relatively small since they correspond to asymmetric vibrations of the ATF, for which the displacement within the region close to the earcanal is not significant. In general, the earcanal lateral walls do not play an important role in the power transfers through the earcanal cavity (blue curve) except at some resonance frequencies of the ATF (i.e., around 2.2 and 4.7 kHz). For the reader's convenience, the principal modal behaviors discussed in Secs. IV B 1 and IV B 2 that affect the power balances in the system, are summarized in Table III.

In the DHP configuration [see Fig. 7(b)], a majority of the power injected into the earcanal cavity at frequencies between 450 Hz and 3.6 kHz originates from its terminal surface, i.e., the SB transmission is dominant. As expected, the highest power injected through this boundary is observed around 2.2 kHz as a result of the ATF mode. Most of the injected power flows out of the earcanal cavity through the earplug medial surface (dashed red curve). Conversely, in the frequency ranges below 450 Hz and above 3.6 kHz, power enters the earcanal cavity mainly through the earplug medial surface (AB transmission dominates). This phenomenon is due to either the earmuff mechanical resonances below 450 Hz (i.e., pumping motion and transverse motion of the silicone cushion) or the acoustic resonance controlled by the earmuff cavity around 4.1 kHz (see Sec. IV A 1), which increases the sound pressure under the earmuff and makes power flow into the earplug directly through its outer surface. Particularly around 4.7 kHz, another bending wave mode of the ATF coincides with an acoustic resonance of the earmuff. These behaviors facilitate the power transmission into the earplug by both the earplug/earcanal walls interface and earplug outer surface [see Fig. B.1(b) in the supplementary material<sup>28</sup>], and

TABLE III. System principal modal behaviors on ATF#1 and ATF#2.

Components (DHP/ATF#1)	Dominant behaviors	Frequency (kHz)
Earmuff	Pumping motion	0.23
	Transverse motion of the silicone cushion	0.38
	Acoustic resonances controlled by the earmuff cavity	4.1 & 4.7
Earplug	Longitudinal vibration of the earplug non-inserted part	1
	Longitudinal vibration of the earplug inserted part	2.5
ATF#1	Symmetric bending wave mode	2.2
	Asymmetric bending wave modes	1.3, 2.9, 4.7 & 4.9
Components (DHP/ATF#2)	Dominant behaviors	Frequency (kHz)
Earmuff/skin assembly	Pumping motion	0.2
	Transverse motion of the silicone cushion	0.3
	Acoustic resonances controlled by the earmuff cavity	4.1 & 4.7
Earplug/skin assembly	Coupled mode controlled by the earplug vibration	0.35
	Multiple coupled modes controlled by the skin vibration	Around 0.8
ATF#2	Symmetric bending wave mode	2
	Asymmetric bending wave mode	1.2

thus increase the power entering the earcanal cavity through the earplug medial surface. Again, the earcanal lateral walls do not significantly contribute to the power in the earcanal cavity. It is important to note that even though the main boundaries for the power injected into the earcanal cavity are switched in the single and DHP configurations, their contributions are comparable in terms of power levels in the frequency range studied.

The power balance in ATF#1 for the DHP configuration is displayed in Fig. 8. Numbers 1–7 denote, respectively, the power spectra levels exchanged between (1) the silicone cushion and ATF, (2) the ATF exterior boundaries outside the earmuff and external air, (3) the microphone holder and ATF, (4) the earcanal lateral walls and earcanal cavity, (5) the earcanal walls and earplug, (6) the ATF boundaries under the earmuff and earmuff cavity, and (7) the power spectrum level dissipated in the ATF.

Two main regimes can be identified from the power balance in ATF#1. First, below about 1 kHz, power mainly flows into the ATF from the silicone cushion (solid red curve), and most of it is radiated into the external air domain through the ATF exterior boundaries (dashed blue curve). This behavior is probably due to the fact that the system is governed by the earmuff mechanical resonances controlled by the silicone cushion, which promotes the vibration transmission from the cushion to the ATF. It is worth noting that in this frequency range, a non-negligible amount of power also gets into the ATF through its boundaries under the earmuff (solid black curve). As explained before, the earmuff

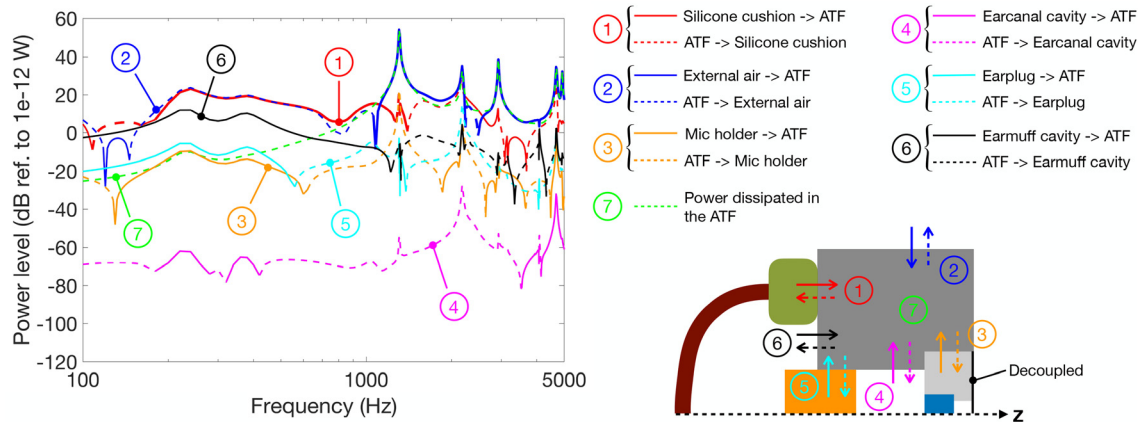


FIG. 8. (Color online) Power balance in ATF#1 for the DHP configuration: power spectra levels exchanged at the silicone cushion/ATF interface (red); exchanged at the ATF exterior boundaries outside the earmuff (blue); exchanged at the microphone holder/ATF interface (orange); exchanged at the earcanal lateral walls (purple); exchanged at the earplug/earcanal walls interface (cyan); exchanged at the ATF boundaries under the earmuff (black); dissipated in the ATF (green). Numbers 1–7 correspond to the associated geometric zones where the powers are calculated. Solid line, power flowing into the ATF; dashed line, power flowing out of (or dissipated in) the ATF.

resonances concurrently raise the sound pressure under the earmuff, and thus the power transmitted into the ATF from the earmuff cavity.

Second, at frequencies above 1 kHz, the exterior boundaries emerge as the dominant ones for the power injected into the ATF (solid blue curve). In this frequency range, the bending wave modes of the ATF are excited (i.e., around 1.3, 2.2, 2.9, 4.7, and 4.9 kHz). They increase the power transmitted into the ATF directly from the external air domain. Most of the power is dissipated in the ATF (dashed green curve). Around certain ATF resonance frequencies (i.e., 2.2 and 4.7 kHz), the injected power flows from the ATF into the silicone cushion (dashed red curve). The remaining part of power is redirected towards other

surrounding domains, such as the earplug, earcanal cavity, and microphone holder. More power is found transmitted from the ATF into the microphone holder around 2.2 kHz (dashed orange curve). This is consistent with the results shown in Fig. 7(b). In the case of ATF#1 with “rigid” earcanal lateral walls, the power exchanged at the earcanal walls (purple curve) is found to be of minor importance in comparison to the total injected power.

## 2. ATF#2: ATF with artificial skin

Similar to Sec. IV B 1, the calculated power balances in the earcanal cavity and ATF#2 are presented respectively in Figs. 9 and 10. In the single earplug configuration

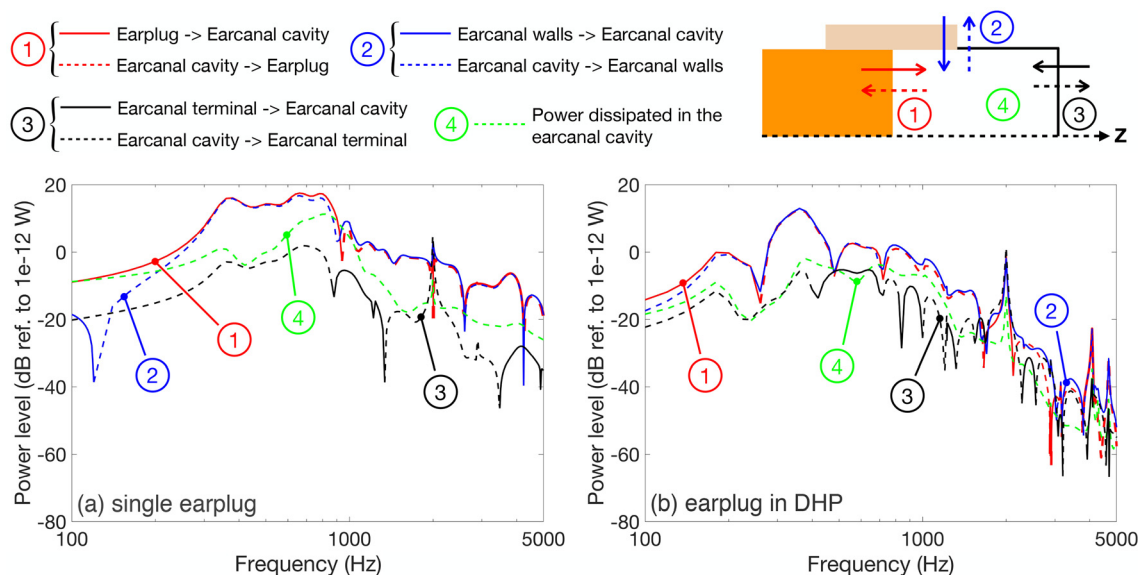


FIG. 9. (Color online) Power balances in the earcanal cavity of ATF#2 for (a) single earplug configuration and (b) DHP configuration: power spectra levels exchanged at the earplug/earcanal cavity interface (red); exchanged at the earcanal lateral walls (blue); exchanged at the earcanal terminal surface (black); dissipated in the earcanal cavity (green). Numbers 1–4 correspond to the associated geometric zones where the powers are calculated. Solid line, power flowing into the earcanal cavity; dashed line, power flowing out of (or dissipated in) the earcanal cavity.



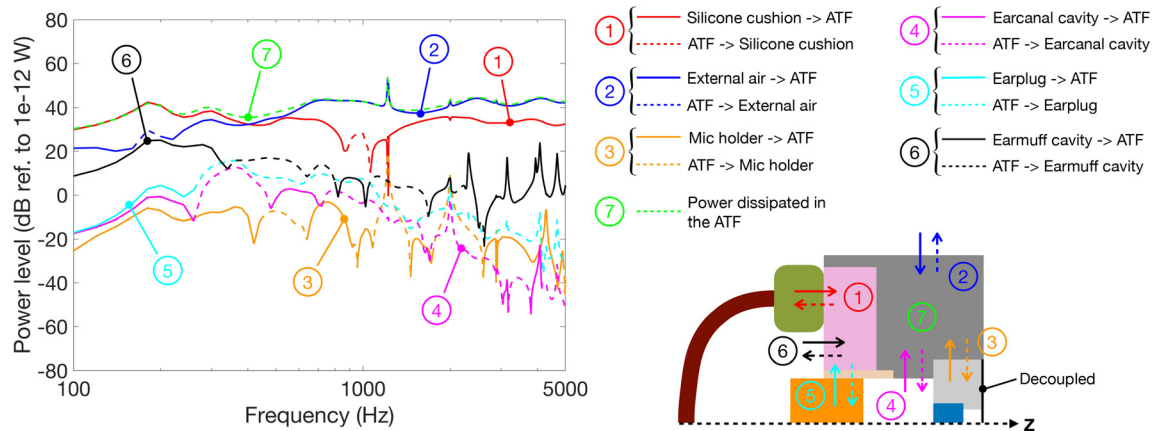


FIG. 10. (Color online) Power balance in ATF#2 for the DHP configuration: power spectra levels exchanged at the silicone cushion/ATF interface (red); exchanged at the ATF exterior boundaries outside the earmuff (blue); exchanged at the microphone holder/ATF interface (orange); exchanged at the earcanal lateral walls (purple); exchanged at the earplug/earcanal walls interface (cyan); exchanged at the ATF boundaries under the earmuff (black); dissipated in the ATF (green). Numbers 1–7 correspond to the associated geometric zones where the powers are calculated. Solid line, power flowing into the ATF; dashed line, power flowing out of (or dissipated in) the ATF.

[see Fig. 9(a)], the earplug medial surface remains the primary boundary for the power injected into the earcanal cavity as on ATF#1 at frequencies below 900 Hz, or between 2.5 and 4 kHz (solid red curve). The highest levels of the injected power are detected around 350 and 800 Hz, which could correspond to the coupled modes of the earplug/skin assembly (see Sec. IV A 2). At about 350 Hz, the coupled mode is dominated by the vibration of the earplug that exhibits the highest displacement. Around 800 Hz, the skin shows the highest displacement, and most power in the earplug is found to come from the earplug/earcanal walls interface [see also Fig. B.2(a) in the supplementary material<sup>28</sup>]. The remaining power in the earcanal cavity is dissipated internally (dashed green curve), and mostly transferred into the ATF through the earcanal lateral walls (dashed blue curve). It is necessary to note that compared to ATF#1, the power injected through the earplug medial surface is approximately 20–60 dB higher in the related frequency ranges on ATF#2. At frequencies between 900 Hz and 2.5 kHz, or above 4 kHz, a pronounced contribution of the earcanal lateral walls to the power in the earcanal cavity is observed when the skin is accounted for (solid blue curve). This observation agrees with the finding of Viallet *et al.*,<sup>10</sup> who considered a skin layer for predicting the sound attenuation of single earplugs inserted into an ATF earcanal. The power injected through the earcanal walls mainly flows out of the earcanal cavity *via* the earplug medial surface (dashed red curve). In opposition to ATF#1, generally no significant contribution of the earcanal terminal surface is found. Particularly around 2 kHz where the symmetric bending wave mode of ATF#2 occurs (see Sec. IV A 2), both the earplug medial surface and earcanal walls are found to transmit power into the earcanal cavity. At this frequency, the terminal surface turns to be an important boundary through which power flees the earcanal cavity (dashed black curve).

In the DHP configuration [see Fig. 9(b)], power mainly flows into the earcanal cavity through the earplug medial surface at frequencies below about 300 Hz (AB transmission dominates). This phenomenon is due to the earmuff pumping motion shifted to around 200 Hz when the artificial skin pad is accounted for, which increases the sound pressure under the earmuff and the power transmitted into the earplug from the earmuff cavity as explained earlier. The injected power is mostly transferred out of the earcanal cavity through its lateral walls. A similar phenomenon is observed around 4.1 kHz where an acoustic resonance of the earmuff takes place (see Sec. IV A 1).

However, in most frequency bands studied, power mainly enters the earcanal cavity through its lateral walls (SB transmission dominates). At frequencies around 350 Hz, or between 750 Hz and 1.6 kHz, the coupled modes of the earplug/skin assembly seem to facilitate the entry of power through the earcanal walls and the exit of power through the earplug medial surface. Similar to the single earplug configuration, both the earplug medial surface and earcanal walls transmit power into the earcanal cavity around 2 kHz. Particularly at this frequency, the power transmitted through the earplug medial surface mostly originates from the earplug/earcanal walls interface [see Fig. B.2(b) in the supplementary material<sup>28</sup>]. The local maximum of the power injected into the earcanal cavity through its surrounding walls at about 4.7 kHz could be explained by another resonance controlled by the earmuff cavity, which increases the direct acoustic excitation on the skin boundaries under the earmuff, and thus the sound radiation of the skin into the earcanal cavity. In general, the power dissipation and earcanal terminal surface are involved to a relatively lesser extent in the power transfers through the earcanal cavity compared to the other boundaries considered.

Similar to ATF#1, the power balance in ATF#2 exhibits two major regimes (see Fig. 10). First, below about 400 Hz,



the silicone cushion emerges as the major source for the power injected into the ATF (solid red curve). Besides the pumping motion which takes place at about 200 Hz, another earmuff resonance governed by the silicone cushion transverse motion is shifted to around 300 Hz. They naturally facilitate the vibration transmission from the cushion to the ATF. In the same frequency band, a noticeable amount of power also gets into the ATF through its exterior boundaries outside the earmuff, especially between 300 and 400 Hz (solid blue curve).

Second, the power injected through the ATF exterior boundaries becomes dominant at frequencies above 400 Hz. The highest level of the power injected through these boundaries is observed around another resonance frequency of ATF#2 at 1.2 kHz. It should be noted that at 1.5 kHz and above, a non-negligible amount of power still flows into the ATF from the silicone cushion. In the whole frequency range of interest up to 5 kHz, the injected power is mostly dissipated in the ATF (dashed green curve), probably due to the presence of the artificial skin, which increases the overall damping of the system. The power transmitted through the other boundaries appears to be less important and is roughly 50–60 dB lower than the injected power in terms of power levels.

### 3. Summary on power balances

The previous observations generally show that for the single earplug configuration on ATF#1, power mainly flows from the earplug into the earcanal cavity through the direct AB sound path in the frequency range of interest. When the earmuff is worn in combination, the DHP effect occurs at frequencies between 450 Hz and 3.6 kHz (see also Fig. 6). In this frequency range, the sound pressure at the earcanal entrance is low due to a relatively high earmuff attenuation, and a significant amount of SB sound power is transmitted from the silicone cushion and ATF exterior boundaries into the earcanal cavity *via* the microphone holder. At frequencies below 450 Hz and above 3.6 kHz, the DHP effect tends to be negligible as the acoustic and mechanical resonances of the earmuff lead to an increase in the sound pressure at the earcanal entrance.

The power balances for ATF#2 highlight the important contribution of the earcanal lateral walls to the power in the earcanal cavity when the artificial skin is accounted for, even in the single earplug configuration at frequencies between 900 Hz and 2.5 kHz, or above 4 kHz. In the DHP configuration, the power in the earcanal cavity is dominated by the sound radiation of its lateral walls, especially at frequencies between 300 Hz and 4 kHz, again due to the SB sound power injected from the silicone cushion and ATF boundaries. This observation agrees with the significant DHP effect observed in the associated frequency range in Fig. 6. Moreover, an indirect SB sound path can be identified at frequencies between 500 and 700 Hz, or around 2 kHz, which corresponds to the sound radiation of the earplug excited by the surrounding earcanal walls. At

frequencies below 300 Hz and above 4 kHz, the DHP effect is not significant as the earmuff resonances raise the direct acoustic excitation on the earplug outer surface and skin boundaries under the earmuff, which makes the AB sound transmission dominant over the SB one.

Additionally, the comparison between the power balances for ATF#1 and ATF#3 [see Figs. B.3–B.5 in the supplementary material<sup>28</sup>] reveals that blocking the acoustic excitation on the ATF exterior boundaries in the DHP configuration generally leads to a lower amount of power injected into the ATF, and thus a relatively smaller contribution of SB sound transmission (i.e., earcanal lateral walls and terminal surface) to the power in the earcanal cavity especially between 450 Hz and 1 kHz, or above 3 kHz. This behavior explains why the DHP effect is mainly observed in the frequency range between 1 and 3 kHz on ATF#3 (see Fig. 6). The power injected into ATF#3 mostly comes from its boundaries under the earmuff at frequencies below 800 Hz and from the silicone cushion at higher frequencies.

Compared to ATF#2, ATF#4 shows no significant overall differences in the power exchanged at the earcanal walls or earplug/earcanal walls interface (in terms of power levels and hierarchization of the boundaries) maybe for the reason that the presence of the skin greatly elevates the contribution of SB transmission, even without the acoustic excitation on the ATF exterior boundaries [see Figs. B.6–B.8 in the supplementary material<sup>28</sup>]. An exception is found around the ATF resonance frequency at 2 kHz, where the power injected through these boundaries is somehow reduced in the DHP configuration. Besides, the decoupled conditions on the ATF boundaries also decrease the power exchanged at the earcanal terminal surface, which is, however, involved to a lesser extent in the power transfers through the system. This finding is consistent with the similar DHP effects observed on ATF#2 and ATF#4 (see Fig. 6). It is interesting to note that the SB power injected into ATF#4 mainly comes from the silicone cushion in the whole frequency range studied.

### C. Discussion

The numerical simulations in the present paper confirm some main conclusions drawn from the authors' previous experimental work.<sup>2</sup> First, the DHP effect indeed originates from the SB sound transmission through the system and can be explained by the relative contributions of the direct AB path and SB paths involved. Second, the sound radiation of the earcanal lateral walls or that of the earplug excited by the earcanal walls constitutes a primary contributor to the sound pressure in the earcanal cavity (when ATF#2 and ATF#4 with the skin are considered). However, the contributions of these boundaries may vary with the earplug insertion depth which can alter the interaction between the earcanal walls and earplug, or between the earcanal walls and earcanal cavity. Third, the earmuff cushion emerges as an important source for the SB sound power injected into the system. These conclusions depend certainly on the

construction of the system (e.g., assembly, materials, and boundary conditions) and frequency range studied as demonstrated in this work.

It should be kept in mind that compared to a commercial ATF or a human head, the simplifications made for the in-house ATF can influence the DHP effect observed. First, the ear simulator in the earcanal of a commercial ATF plays an important dissipative role,<sup>10</sup> and may evidently reduce the sound radiation of the earcanal terminal surface in ATF#1 and ATF#3. Second, the human middle ear ossicular resonances above 1 kHz<sup>29</sup> are expected to increase the mid-frequency contribution of the earcanal terminal portion to the power injected into the earcanal cavity. Additionally, Berger *et al.*<sup>4</sup> have achieved additional gains in the measured DHP attenuation at frequencies above 1–2 kHz when shielding the human head from acoustic stimulation, whereas for the simulation configurations with the skin (i.e., ATF#2 and ATF#4), blocking the acoustic excitation on the ATF exterior boundaries does not lead to significant overall differences in the SB transmission or DHP effect. This analysis suggests that more realistic modifications need to be made to the system for better capturing the DHP attenuation on human subjects. However, despite some limitations, the present paper has demonstrated the use of a computational model for predicting the DHP effect on an ATF, which also helps understand the related physical mechanisms. The model can be further improved by increasing the complexity of the system in terms of geometry and material properties for ultimately studying the DHP effect on human subjects.

## V. CONCLUSION

In the present paper, a FE model has been proposed in order to study the DHP effect on an in-house ATF. This effect has been characterized by the difference between the NRs of the earplug alone and in the DHP. The comfort cushion of the earmuff was replaced by a silicone cushion to better capture its vibroacoustic behavior in the model. First, the simulation results based on the model have been compared with the NR measurements of the single earmuff, single earplug, and earplug in the DHP in the frequency range between 100 Hz and 5 kHz. The model has been found to closely reproduce the sound attenuation of the earmuff and earplug used independently, and to capture the system's overall behavior in a satisfactory manner when the two are used in combination. The contact conditions between the ATF components could be further improved in order for the model to better account for the SB sound transmission through the system.

Second, exploited simulation configurations of the ATF have been used to simulate and analyze the power balances in the system for (i) quantifying the contribution of each sound path, and studying the effects of (ii) the artificial skin and (iii) acoustic excitation on the ATF exterior boundaries. On the fully “rigid” ATF, the DHP effect arises between 450 Hz and 3.6 kHz due to a large amount of SB sound

power transmitted into the earcanal cavity through its terminal surface. In other frequency bands, the DHP effect tends to be negligible as the earmuff resonances increase the sound pressure at the earcanal entrance, and make the AB sound transmission through the earplug dominant over the SB one. On the ATF with artificial skin components, the sound radiation of the earcanal lateral walls is proved to be the major cause of the evident DHP effect occurring between 300 Hz and 4 kHz. A relevant indirect SB path can also be identified, which corresponds to the sound radiation of the earplug excited by the earcanal walls. This configuration highlights the importance of taking into account the skin if a more realistic prediction of DHP attenuation is desired. Additionally, the acoustic excitation on the ATF exterior boundaries is found to have a non-negligible influence on the DHP effect captured on the “rigid” ATF especially below 1 kHz or above 3 kHz, whereas it does not significantly affect the DHP effect on the ATF with the skin. The SB power injected into the system is shown to mainly come from the earmuff silicone cushion and/or ATF boundaries depending on the materials, boundary conditions and frequency range studied. This work has allowed for gaining more insight into the sound transmission mechanisms through a DHP/ATF system. Prospectively, it will also provide a useful tool for more realistic DHP attenuation predictions based on legitimate increases in the system complexity.

## ACKNOWLEDGMENTS

The authors wish to acknowledge the Natural Sciences and Engineering Research Council of Canada (NSERC) for funding this research.

## APPENDIX: YOUNG'S MODULUS AND LOSS FACTOR OF THE SILICONE CUSHION

The fractional derivative Zener model is defined in Eq. (A1). In this model,  $M(f)$  denotes the complex-valued stiffness,  $M_0$  denotes the static stiffness,  $M_\infty$  is the high frequency limit of the stiffness,  $\alpha$  is an exponent ( $0 < \alpha < 1$ ), and  $t_r$  refers to a relaxation time. The model parameters obtained by curve fitting the QMA data are given in Table IV. The frequency dependent Young's modulus and loss factor of the silicone cushion are calculated, respectively, by  $E(f) = \Re(M(f))$  and  $\eta(f) = \Im(M(f))/\Re(M(f))$ , and are presented in Fig. 11,

$$M(f) = \frac{M_0 + M_\infty (j2\pi f t_r)^\alpha}{1 + (j2\pi f t_r)^\alpha}. \quad (\text{A1})$$

TABLE IV. Mechanical properties of the silicone cushion (fractional derivative Zener model).

$\alpha$ (1)	$M_0$ (Pa)	$M_\infty$ (Pa)	$t_r$ (s)
0.290 68	101 469	958 471	$9.89 \times 10^{-7}$

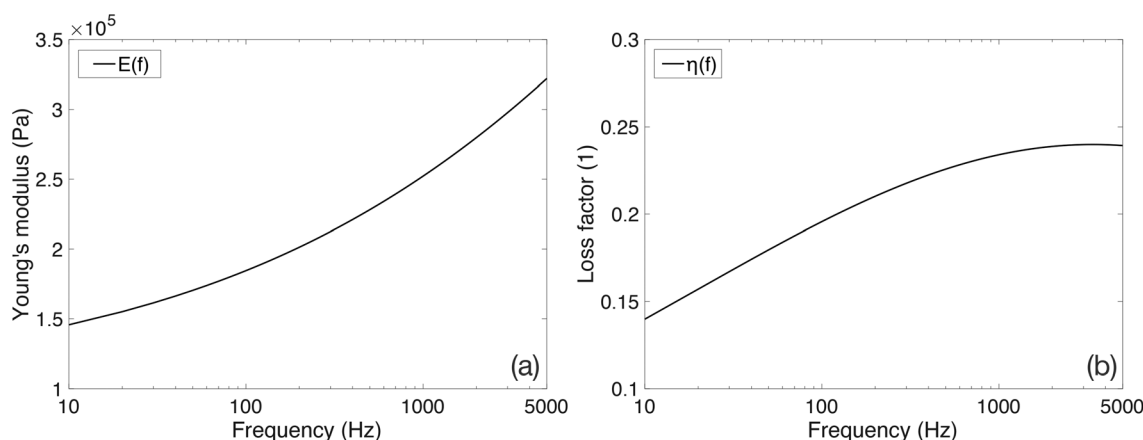


FIG. 11. (a) Young's modulus and (b) loss factor of the silicone cushion.

<sup>1</sup>CSA-Z94.2-14: *Hearing Protection Devices: Performance, Selection, Care and Use* (Canadian Standards Association, Toronto, Canada, 2014).

<sup>2</sup>Y. Luan, O. Doutres, H. Nélisse, and F. Sgard, "Experimental study of earplug noise reduction of a double hearing protector on an acoustic test fixture," *Appl. Acoust.* **176**, 107856 (2021).

<sup>3</sup>E. H. Berger, "Laboratory attenuation of earmuffs and earplugs both singly and in combination," *Am. Ind. Hygiene Assoc. J.* **44**(5), 321–329 (1983).

<sup>4</sup>E. H. Berger, R. W. Kieper, and D. Gauger, "Hearing protection: Surpassing the limits to attenuation imposed by the bone-conduction pathways," *J. Acoust. Soc. Am.* **114**(4), 1955–1967 (2003).

<sup>5</sup>S. E. Mercy, C. Tubbs, and S. H. James, "Experimentation to address appropriate test techniques for measuring the attenuation provided by double ANR hearing protectors," in *New Directions for Improving Audio Effectiveness Meeting Proceedings RTO-MP-HFM-123*, Neuilly-sur-Seine, France (April 14, 2005), Paper 1.8.

<sup>6</sup>C. Tubbs, S. E. Mercy, and S. H. James, "Investigating double hearing protection using human subjects," in *New Directions for Improving Audio Effectiveness Meeting Proceedings RTO-MP-HFM-123*, Neuilly-sur-Seine, France (April 14, 2005), Paper 19.

<sup>7</sup>S. Stenfelt and R. L. Goode, "Bone-conducted sound: Physiological and clinical aspects," *Otology Neurotol.* **26**(6), 1245–1261 (2005).

<sup>8</sup>H. Nélisse, F. Sgard, M.-A. Gaudreau, and T. Padois, "Attenuation of dual hearing protection: Measurements and finite-element modeling," *J. Acoust. Soc. Am.* **141**(5), 3633 (2017).

<sup>9</sup>G. Viallet, F. Sgard, F. Laville, and J. Boutin, "Axisymmetric versus three-dimensional finite element models for predicting the attenuation of earplugs in rigid walled ear canals," *J. Acoust. Soc. Am.* **134**(6), 4470–4480 (2013).

<sup>10</sup>G. Viallet, F. Sgard, F. Laville, and J. Boutin, "A finite element model to predict the sound attenuation of earplugs in an acoustical test fixture," *J. Acoust. Soc. Am.* **136**(3), 1269–1280 (2014).

<sup>11</sup>S. Boyer, O. Doutres, F. Sgard, F. Laville, and J. Boutin, "Low frequency finite element models of the acoustical behavior of earmuffs," *J. Acoust. Soc. Am.* **137**(5), 2602–2613 (2015).

<sup>12</sup>K. Carillo, F. Sgard, and O. Doutres, "Numerical study of the broadband vibro-acoustic response of an earmuff," *Appl. Acoust.* **134**, 25–33 (2018).

<sup>13</sup>C. James, "Finite element modeling and exploration of double hearing protection systems," M.S. thesis, Virginia Polytechnic Institute and State University, Blacksburg, VA (2006).

<sup>14</sup>ANSI/ASA S12.42: *Methods for the Measurement of Insertion Loss of Hearing Protection Devices in Continuous or Impulsive Noise Using Microphone-in-Real-Ear or Acoustic Test Fixture Procedures* (American National Standards Institute, New York, 2020).

<sup>15</sup>IEC 60318-4: *Simulators of Human Head and Ear-Part 4: Occluded-Ear Simulator for the Measurement of Earphones Coupled to the Ear by Means of Ear Inserts* (International Electrotechnical Commission, Geneva, Switzerland, 2010).

<sup>16</sup>Y. Luan, F. Sgard, S. Benacchio, H. Nélisse, and O. Doutres, "A transfer matrix model of the IEC 60318-4 ear simulator: Application to the

simulation of earplug insertion loss," *Acta Acust. united Ac.* **105**(6), 1258–1268 (2019).

<sup>17</sup>S. Stenfelt and S. Reinfeldt, "A model of the occlusion effect with bone-conducted stimulation," *Int. J. Audiol.* **46**(10), 595–608 (2007).

<sup>18</sup>H. Bériot and G. Gabard, "Anisotropic adaptivity of the p-FEM for time-harmonic acoustic wave propagation," *J. Comput. Phys.* **378**, 234–256 (2019).

<sup>19</sup>N. Atalla and F. Sgard, *Finite Element and Boundary Methods in Structural Acoustics and Vibration* (CRC Press, Boca Raton, FL, 2015).

<sup>20</sup>W. R. Kampinga, "Viscothermal acoustics using finite-elements—Analysis tools for engineers," Ph.D. thesis, University of Twente, Enschede, the Netherlands (2010).

<sup>21</sup>ISO 18437-5: *Mechanical Vibration and Shock – Characterization of the Dynamic Mechanical Properties of Visco-Elastic Materials – Part 5: Poisson Ratio Based on Comparison between Measurements and Finite Element Analysis* (International Organization for Standardization, Geneva, Switzerland, 2011).

<sup>22</sup>F. Sgard, N. Atalla, and J. Nicolas, "A numerical model for the low frequency diffuse field sound transmission loss of double-wall sound barriers with elastic porous linings," *J. Acoust. Soc. Am.* **108**(6), 2865–2872 (2000).

<sup>23</sup>S. Boyer, O. Doutres, F. Sgard, F. Laville, and J. Boutin, "Objective assessment of the sound paths through earmuff components," *Appl. Acoust.* **83**, 76–85 (2014).

<sup>24</sup>S. Boyer, "Étude de la transmission sonore à travers un protecteur de type 'coquilles': Modélisation numérique et validation expérimentale" ("Study of the sound transmission through earmuffs: Numerical modeling and experimental validation"), Ph.D. thesis, École de Technologie Supérieure, Montreal, Canada (2015).

<sup>25</sup>E. H. Berger, L. H. Royster, J. D. Royster, D. P. Driscoll, and M. Layne, *The Noise Manual*, 5th ed. (American Industrial Hygiene Association, Fairfax, VA, 2003), pp. 391–397.

<sup>26</sup>R. Pääkkönen, "Effects of cup, cushion, band force, foam lining and various design parameters on the attenuation of earmuffs," *Noise Control Eng. J.* **38**(2), 59–65 (1992).

<sup>27</sup>F. Sgard, H. Nélisse, M.-A. Gaudreau, J. Boutin, J. Voix, and F. Laville, "Étude de la transmission sonore à travers les protecteurs auditifs et application d'une méthode pour évaluer leur efficacité en milieu de travail—Partie 2: Étude préliminaire d'une modélisation par éléments finis" ("Study of the sound transmission through hearing protection devices and application of a method for evaluating their real efficiency in the workplace—Part 2: Preliminary study of finite element modeling"), Report R-680 (IRSST, Montreal, Canada, 2010).

<sup>28</sup>See supplementary material at <https://www.scitation.org/doi/suppl/10.1121/10.0009835> for the simulated power balances in the earplug, and for ATF#3 and ATF#4.

<sup>29</sup>P. V. Brüel, E. Frederiksen, H. Mathiasen, G. Rasmussen, and E. Sigh, "Impedance of real and artificial ears-Part I: Investigations of a new insert earphone coupler," Technical Report (Brüel & Kjær, Naerum, Denmark, 1976).